Formation of Air Stable Graphene p–n–p Junctions Using an Amine-Containing Polymer Coating

*Hossein Sojoudi, Jose Baltazar, Laren Tolbert, Clifford Henderson, and Samuel Graham**

An ultrathin layer of a polymer containing simple aliphatic amine groups, polyethylenimine ethoxylated (PEIE), is deposited on a back-gated field effect graphene device to form graphene p–n–p junctions. Characteristic I–V curves indicate the superposition of two separate Dirac points, which confirms an energy separation of neutrality points within the complementary regions. This is a simple approach for making graphene p–n–p junctions without a need for multiple lithography steps or electrostatic gates and, unlike, the destructive techniques such as substitutional doping or covalent functionalization, it induces a minor defect, if any, as there is no discernible D peak in the Raman spectra of the graphene films after creating junctions and degradation in the charge carrier mobilities of the graphene devices. This method can be easily processed from dilute solutions in environmentally-friendly solvents such as water or methoxyethanol and does not suffer any change upon exposure to air or heating at temperatures below 100 °C.

1. Introduction

Graphene has many unique electrical properties, including its nearly linear energy dispersion relation, which results in electric-field-induced generation of electrons and holes in the material. These electrons theoretically travel as massless Dirac fermions with very high velocities.[1–5] Due to the zero-gap in single-layer graphene, both carrier type and concentration can be controlled through an electrostatic gate, making graphene a promising material for semiconductor applications.[1,3] Graphene junctions in which exciting phenomena such as Klein tunneling[6] and fractional quantum Hall transport[7] have been studied and observed, can be formed using this electrostatic gating. Most of the studies reported so far on the formation of graphene junctions have used multiple electrostatic gates,[7,8] electrical stress-induced doping,[9] chemical treatment by gas exposure,[10] molecular modifications on top of the graphene,[11–13] ionic liquid gating,[14] local doping by focused laser irradiation[15] and deep UV radiation,[16] and modification of the substrate by changing the local electrostatic potential in the vicinity of one of the contacts.[17,18] However, these methods might not be stable and can degrade carrier mobility by introducing defects. A low-temperature method was recently developed to fabricate junctions in graphene by modifying the interface between graphene and its support substrate with covalently bonded self-assembled monolayers (SAMs).[19,20] P- and n-type SAMs were patterned on a field effect transistor (FET) device, resulting in thermally stable graphene junctions while minimizing the introduction of defects.[19,20] However, these junctions are not stable upon exposure to air requiring hermetic packaging and multiple lithography steps to pattern a graphene FET channel.

Here, we utilize an ultrathin layer of a polymer containing simple aliphatic amine groups, polyethylenimine ethoxylated (PEIE), on a back-gated FET device to obtain graphene p–n–p junctions. Recently, PEIE was employed as a universal method to lower the work function (WF) of conductors including metals, transparent conductive metal oxides, conducting polymers, and graphene.[21] Amine-terminated compounds were shown to be effective molecules to control doping in graphene films.[19,20] In contrast to π-conjugated amine-containing small molecules and polymers, PEIE is an insulator, and it should not be regarded as a charge injection layer but rather as a surface modifier. The intrinsic molecular dipole moments associated with the neutral amine groups contained in such an insulating polymer layer, and the charge-transfer character of their interaction with the conductor surface, together reduce the WF of graphene.[21] In contrast, gold, a well-known electron acceptor,[22] results in p-doping of graphene. Charge transfer at a metal–graphene interface results in doping of the graphene sheet due to differences in the WFs.[23–27] In physisorption interfaces such as those in graphene/gold contact, Fermi level pinning and Pauli-exclusion-induced energy-level shifts are shown to be two primary factors determining graphene's doping types and densities.[17,28–30] Thus, adding a layer of PEIE on a back-gated graphene FET device with gold contacts results in formation of graphene regions with n- and p-type characteristics on a single FET device.

Dr. H. Sojoudi, Prof. S. Graham
Woodruff School of Mechanical Engineering
Georgia Institute of Technology
Atlanta, Georgia 30332, USA
E-mail: sgraham@gatech.edu
Dr. J. Baltazar, Prof. C. Henderson
School of Chemical & Biomolecular Engineering
Georgia Institute of Technology
Atlanta, Georgia 30332, USA
Prof. L. Tolbert
School of Chemistry & Biochemistry
Georgia Institute of Technology
Atlanta, Georgia 30332, USA

DOI: 10.1002/admi.201400378

© 2014 WILEY-VCH Verlag GmbH & Co. KGaA, Weinheim

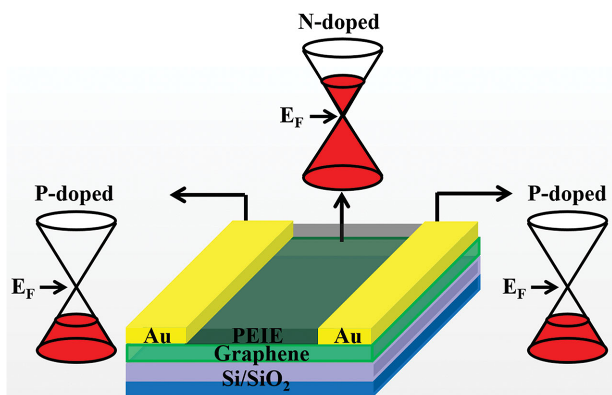

Figure 1. Schematic of the graphene p–n–p junction using PEIE.

2. Results and Discussion

Figure 1 schematically illustrates the formation of graphene p–n–p junctions using PEIE. Monolayer graphene was grown on a Cu foil and transferred onto highly doped Si substrates coated with 300 nm thick SiO_2 layer (see Experimental Section for details). The samples were then annealed in an inert environment at 200 °C overnight to remove any species that might be chemically and/or physically adsorbed on the graphene during the transfer process.[31] Lithography and plasma etching were used to define a channel; the source and drain contacts (50 nm Au deposited through E-beam evaporation) were defined using conventional photolithography and lift-off processes. PEIE (Mw = 70 000 g mol^{-1}), received from Aldrich, was dissolved in H_2O with a concentration of 35–40 wt%. It was further diluted with 2-methoxyethanol (hereafter referred to as methoxyethanol) to a weight concentration of 0.4%[21] and then deposited on the channel though spin coating (5000 rpm for 1 min resulted in PEIE thickness of ≈10 nm).[21] The resulting channel size was 50 µm wide and 2 mm long. For X-ray photoelectron spectroscopy (XPS) and Kelvin probe measurements, graphene, and PEIE coated graphene samples on SiO_2 substrates were made similarly without device fabrication. The thickness of these PEIE layers was determined to be around 10 nm by spectroscopic ellipsometry measurements (J. A. Woollam Co.).

2.1. Characteristic Study of Graphene p–n–p Junctions

Atomic force microscopy (AFM, Dimension 3100 Multimode AFM, NanoScope III controller, Veeco) measurements were done on bare and PEIE coated graphene samples. **Figure 2**a shows AFM image of bare graphene and PEIE coated graphene both on SiO_2 substrates over a 20 × 20 µm^2 area. AFM images show uniform coverage of graphene with PEIE film without pin holes. Some inhomogeneity in the thickness of the PEIE film can be seen that is common in deposition of thin films through spin coating.

XPS was employed to confirm the presence of PEIE on graphene samples on SiO_2 substrates. Figure 2a shows survey scan

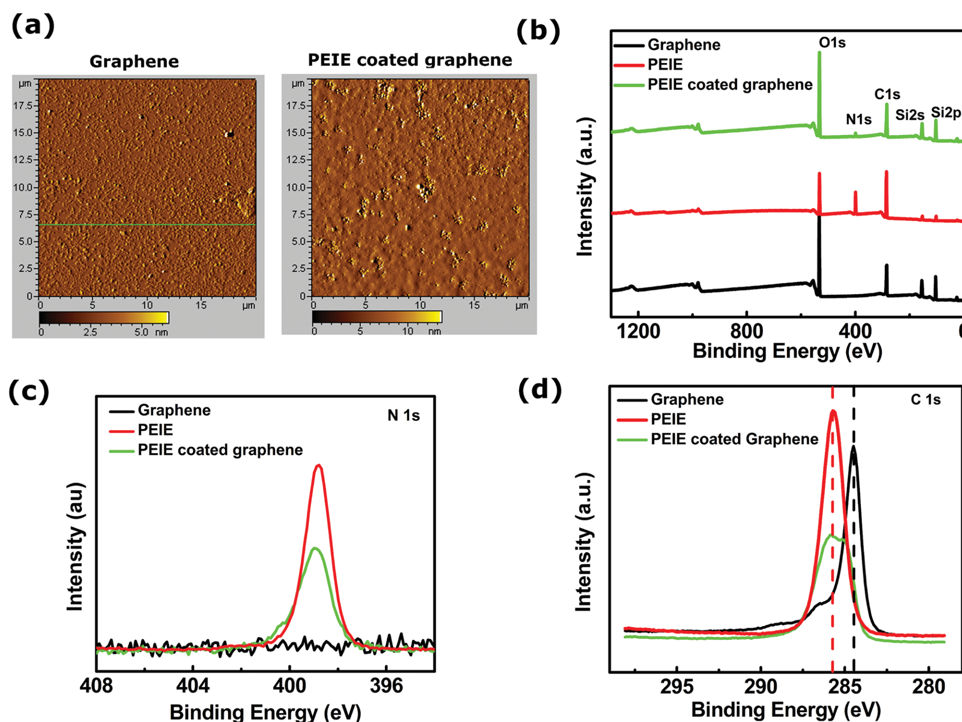

Figure 2. a) AFM images of graphene (left) and PEIE coated graphene (right) acquired in a 20 × 20 µm^2 area. XPS spectra representing b) Survey scan, c) Core level N1s BE and d) Core level C1s BE for graphene on SiO_2 (black), PEIE on SiO_2 (red), and PEIE coated graphene on SiO_2 (green). The C1s XPS spectra of PEIE coated graphene on SiO_2 is a superposition of graphene on SiO_2 and PEIE on SiO_2 C1s spectra, and it confirms that PEIE is present on the graphene film. The presence of N1s BE in (c) and the shift in C1s BE in (d) in PEIE coated graphene verifies n-doping of graphene induced by PEIE.

© 2014 WILEY-VCH Verlag GmbH & Co. KGaA, Weinheim

spectra randomly collected from as-transferred graphene and graphene with PEIE on top. The scan showed the most prominent peaks to be C1s and O1s on all spectra. The appearance of an N1s peak centered at 400.1 eV in the survey spectra confirms the presence of PEIE due to an excess amount of nitrogen-containing amine groups. High-resolution XPS spectra of N1s were obtained over 389–401 eV with a step size of 0.1 and 50 eV pass energy; these indicate that the concentration of nitrogen in the as-made graphene device is below the detection limit of XPS. A high-resolution XPS spectrum of the C1s binding energy (BE) was also acquired over 282–293 eV with a similar step size and pass energy. The C1s BE of graphene is centered at 284.5 eV. The C1s BE for PEIE is centered at 285.5 eV, due to the different binding states of carbon atoms in the PEIE structure. The C1s XPS spectrum of the PEIE/graphene is a superposition of the graphene and the PEIE C1s spectra, and it confirms that PEIE is present on the graphene film. The appearance of a shoulder and a shift in the C1s peak position of PEIE coated graphene suggests the n-doping induced by PEIE deposition.[30,32]

2.2. Raman Spectroscopy Study

Raman spectroscopy was acquired in a Renishaw inVia microscope spectrometer to investigate the quality of the graphene and its doping state before and after PEIE and Au deposition by examining the D, G, and 2D bands and their positions. Chemical vapor deposition (CVD) graphene films are intrinsically p-doped due to the presence of chemical groups bounded and/or physically absorbed to graphene during the transfer process.[31] A heat treatment process under an inert atmosphere has been typically employed on CVD graphene films to remove the unintentional dopants in order to fully reveal the effect of intentional dopants.[31] Both graphene FET devices and control graphene samples were heated up to 200 °C under an inert atmosphere and held up to 180 min to allow for desorption of atmospheric p-dopants bonded to the sample, prior to PEIE deposition. It is believed that PEIE film can function as an encapsulating layer to limit any p-doping by exposure to air.[21]

Figure 3a shows Raman spectra of control graphene on SiO_2 substrate and after Au and PEIE deposition on graphene FET devices. The lack of discernible defect band (D band) in Raman spectra of control graphene samples on SiO_2 substrates indicates a successful transfer of CVD graphene without inducing defects. This is important for the devices with very large channels (50 µm × 2 mm) studied in this work. The measurements were performed at multiple spots in each region to verify reproducibility. Average values and standard deviations were generated over these spots. The difference in the G and 2D peak width, position, and their intensity ratio for each device and at different locations is indicative of various doping states.[33–44] A critical observation is that no increase on the D band was observed after PEIE deposition; hence successful doping of the graphene monolayer without significant damage to the lattice structure was achieved.[45,46] The G and 2D peaks' positions before and after PEIE deposition were monitored. Full width at half maximum of G peak, FWHM (G), and intensity ratio of

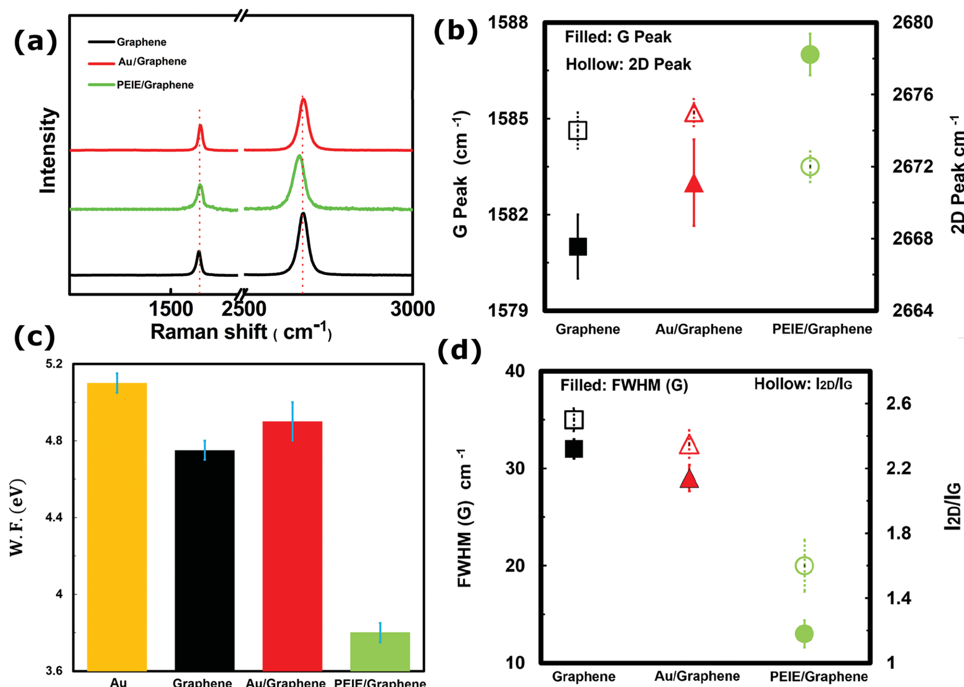

Figure 3. a) Raman spectra of graphene (black), Au/Graphene (red), and PEIE/Graphene (green) all on SiO_2 substrate. b) G and 2D peaks position and d) FWHM (G) and I_{2D}/I_G of Graphene, Au/Graphene, and PEIE/Graphene. The shifts in Raman peak position, linewidth, and intensity ratio verifies p- and n-doping of graphene by Au and PEIE, respectively. c) The WF of bare gold, graphene, Au/Graphene, and PEIE/Graphene. An increase in the WF of graphene by Au and a decrease by PEIE deposition, confirms p- and n-doping, respectively, and verifies the results of Raman spectroscopy measurements.

© 2014 WILEY-VCH Verlag GmbH & Co. KGaA, Weinheim

2D over G peak (I_{2D}/I_G) reveal the changes in electronic state of various spots on graphene FET devices. Figure 3b shows that, for Au/graphene, the G and 2D Raman peaks' positions are 1583 ± 1 cm^{-1} and 2675 ± 0.7 cm^{-1}, respectively. These are higher than the corresponding values for graphene on SiO_2 (G at 1581 ± 0.9 cm^{-1} and 2D at 2674 ± 0.9 cm^{-1}) and are indicative of enhanced p-doping induced by the Au layer. After PEIE deposition, the G peak positions of PEIE/graphene increase ≈6 cm^{-1} while the 2D peaks positions decrease ≈2 cm^{-1}, which is in accord with observed Raman characteristics for n-doped graphene.[33] The shifts in the Raman spectra are in accord with the observed shift in the C1s XPS spectra of graphene after PEIE deposition. Figure 3d shows ≈18 cm^{-1} and ≈0.9 decrease in FWHM (G) and I_{2D}/I_G, respectively, confirms n-doping by PEIE. In addition, ≈4 cm^{-1} and ≈0.2 cm^{-1} decrease in the FWHM (G) and the I_{2D}/I_G, respectively, verifies the p-doping effect by the Au layer. Overall, Raman spectroscopy measurements confirm the presence of graphene with n- and p-type doping states within a single FET device, which is the key for formation of a graphene p–n–p junction.

2.3. Work Function Measurements

The WF was measured by Scanning Kelvin Probe (Besocke Delta Phi) to verify the doping of graphene by PEIE and gold contacts and the shift in their Fermi energy level. The measurements were also performed on bare graphene and bare gold substrates (deposited through E-beam evaporation), resulting in WFs of 4.75 ± 0.05 eV and 5.1 ± 0.05 eV, respectively, which are within the range reported in the literature.[25,26,29,37] Figure 3c shows the changes in the WF of graphene by Au and PEIE layer. As expected, charge transfer at the Au–graphene interface causes p-doping in the graphene sheet due to differences in their WFs resulting in a WF of 4.9 ± 0.1 for Au/graphene. In contrast, the deposition of PEIE on graphene creates intrinsic molecular dipole moments, associated with the neutral amine groups in PEIE, which interacts with conductive graphene resulting in a WF of 3.8 ± 0.05 eV for the PEIE/graphene. This is a significant reduction in the WF of graphene by a simple method which is stable in air. N-doping of graphene has been extensively investigated.[35,47–51] Some methods have shown promise on n-doping of graphene at a whole range of temperatures and are air stable as well. For example, Matis et al. have demonstrated n-doping of graphene by light hydrogenation through the conversion of the majority of carrier type from electrons to holes. However, hydrogenation may not be safe and can induce defects to the structure of the graphene as verified by the appearance of a significant defect peak (D) in the Raman spectra after the treatment.[52,53]

2.4. Electrical Data Measurements

To further demonstrate the n- and p-type characteristics induced by PEIE and Au layers in back-gated FET devices, electrical measurements were performed. Another set of devices was fabricated, without PEIE, as control devices with the same dimensions (50 μm wide and 2 mm long). Electrical transport data was measured on the control and the PEIE coated graphene devices (see **Figure 4**a). The charge neutrality point for control graphene devices was around zero volts, indicative of undoped graphene as shown in Figure 4a. CVD graphene devices are intrinsically p-doped due to the presence of atmospheric dopants mainly induced during the transfer process of CVD graphene.[31] However, heat treatment performed on control and PEIE coated graphene devices removes atmospheric dopants and results in an undoped (de-doped) graphene. For the PEIE coated devices, two Dirac points (peaks) were seen in the I_d–V_{gs} curve: one located at V_{np} ≈ 38 V and the other at V_{np} ≈ −20 V, which indicates an energy separation of the neutrality points within the complementary regions (V_d = 0.1 V). A conductivity asymmetry in the I_d–V_{gs} curve might be attributed to a high doping level in graphene in the vicinity of metal contacts.[54] Density functional theory calculations performed in the contact region have shown that the metal contact can give rise to the formation of a p–p, n–n, and p–n junction or with additional gating or impurity doping, even a p–n–p junction that contributes to the overall resistance of the graphene sample, destroying its electron-hole symmetry.[23,24] In addition, the doping of the graphene by the gold contacts is not limited to only underneath the metal electrodes but extends for 0.2–0.3 μm or longer in the inner channel, since the graphene, having zero density of states at the Dirac point, is not able to absorb all the transferred charge at the interface.[55,56] Comparison of the I_d–V_{gs} curve for the control and the PEIE coated graphene device indicates a significant increase in the current after PEIE deposition. This is due to the significant presence of negative charge carrier concentrations on graphene, induced by the ultrathin layer of PEIE, and it confirms the observed reduction in the WF of graphene.[21] Several control and PEIE coated devices were fabricated, and similar results were obtained for each set of devices. One might compare the observed double Dirac points in the I_d–V_{gs} curve to very sharp and distinct ones observed in graphene junctions reported elsewhere such as those by Avouris and co-workers.[18] They have observed sharp Dirac points only in the vicinity of the contacts due to local electrostatic potential. They have shown that the original Dirac point stays unaffected, while the position of a second Dirac point caused by a drain stress depends on the back-gate voltage. A positive charge that is trapped at the graphene/oxide interface in the vicinity of the drain has induced the formation of a p–n junction in the drain region resulting in sharp and distinct Dirac points.[11,18] Another comparison might relate a double dip in the I_d–V_{gs} curve to partial Fermi energy pinning and charge transfer. These phenomena can be seen in disordered devices, dirty devices, or devices on substrates that have been significantly charged. For example, Bartolomeo et al. have shown the appearance of double Dirac points (two conductance minima) by depositing a 250 nm thick Poly(methyl methacrylate) on a FET device only after applying an electrical gate voltage (V_{gs}) cycles.[57] A second feature observed in their I_d–V_{gs} curves is a clear hysteresis between the forward and reverse sweeps of the gate voltage. In this work, we deposited an ultrathin layer of PEIE (10 nm thick) and observed two distinct Dirac points without any appearance of hysteresis or a need for electrical cycling.[58]

© 2014 WILEY-VCH Verlag GmbH & Co. KGaA, Weinheim

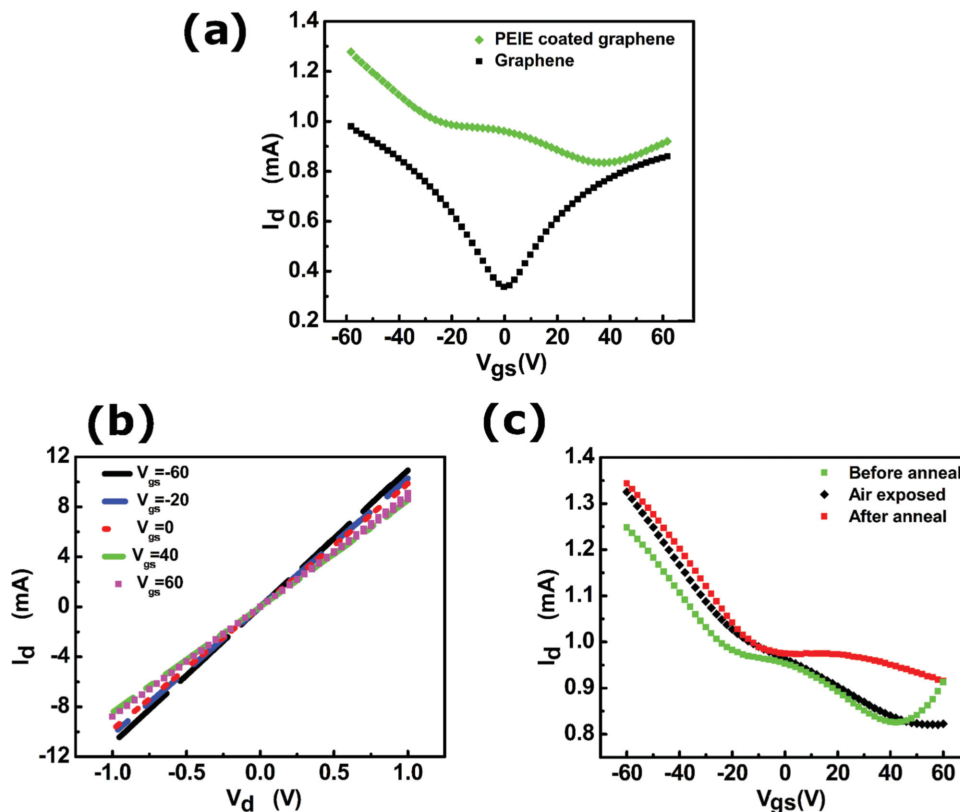

Figure 4. a) Drain-source current versus gate voltage (I_d–V_{gs}) for graphene FET device (black) and PEIE coated graphene FET device (green) at V_d = 0.1 V. b) I_d–V_d characteristic of the PEIE/graphene FET device at different gate voltages which indicates ohmic contacts. c) I_d–V_{gs} of as-made PEIE coated graphene FET device before annealing (green), after air exposure for several days (black), and after annealing up to 100 °C for 30 min (red). The appearance of double Dirac points in I_d–V_{gs} curves after air exposure and annealing suggests that developed graphene p–n–p junctions are thermally and environmentally stable.

Electron and hole field-effect mobilities for graphene devices were ≈4500 ± 600 cm^2 $(Vs)^{-1}$ and ≈5200 ± 800 cm^2 $(Vs)^{-1}$, respectively (averaged over five devices measurements). These values for graphene p–n–p junctions were ≈3900 ± 200 cm^2 $(Vs)^{-1}$ and ≈4300 ± 300 cm^2 $(Vs)^{-1}$ for electron and hole mobilities, respectively, which are of the same order of magnitude as the graphene devices (averaged over five devices measurements) indicating that the PEIE has only a minor effect, if any, on the mobility of graphene devices. These values are extracted using Equation (1):

$$\mu_{FE} = L_{ch} g_m / W_{ch} V_d C_{0x} \quad (1)$$

where L_{ch} = 2 mm, W_{ch} = 50 µm, V_d = 0.1 V, and C_{ox} = 115 aF μm^{-2},[19,59] and $g_m = dI_d/dV_{gs}$ (peak g_m value from the linear regime of the I_d–V_{gs} curve was used for calculating the mobilities). This is in contrast with other methods to form graphene junctions such as those using electrical stressing. At such high-level voltage stressing, the carrier mobility can be degraded, possibly due to short-range scattering caused by deep-level charge trapping near the surface of the SiO_2 substrate under high electric field in the vertical direction.[9] Typically, an increase in the charge carrier concentration via doping can result in a decrease in the mobility due to intrinsic scattering of the carriers. In this work, the slight differences in the mobility of graphene and PEIE coated graphene FET devices can be due to the differences in the transferred graphene that has origins in varying grain size or transfer process of CVD graphene.[60,61]

Figure 4b displays the I_d–V_d output for control and PEIE coated graphene devices at variable back-gate voltages (V_{gs}). The linear I_d–V_d behavior in all devices indicates good ohmic contact at the Au–graphene interface. For a given V_d, an increase in V_{gs} from 40 to 60 V results in an I_d increase indicative of p-type characteristics, and a decrease in V_{gs} from –20 to –60 V causes an increase in I_d, demonstrating n-type characteristics in a single-junction device. Unlike a conventional semiconductor junction, I_d–V_d curves do not show rectifying behavior.[62] This is due to the chirality of the massless Dirac fermions of graphene, which suppresses backscattering by potential barriers (Klein Tunneling).[7] The PEIE thickness on the substrate can be tuned to fully control the transport behavior of the fabricated p–n–p junction. Unlike graphene junctions using electrostatic gating or SAMs, the doping and formation of a p–n–p junction using PEIE is stable upon exposure to heat and atmosphere. Figure 4c compares the I_d–V_{gs} output of a typical as-made p–n–p junction with its performance after exposure to air for several days. It is important to note that the transport measurements were performed without any heat treatment after air exposure. The presence of two separate Dirac points indicates

© 2014 WILEY-VCH Verlag GmbH & Co. KGaA, Weinheim

that the junctions survived and are air stable. This indicates that PEIE film acts as a barrier film and prevents any absorption of atmospheric dopants on graphene. The p–n–p junction devices underwent a heat treatment test as well. To this end, devices were placed on a hotplate at 100 °C for 30 min in atmospheric conditions and the measurements were repeated after the devices were cooled down. I_d–V_{gs} transport data preserve the same trend observed in the as-made p–n–p junctions and indicate that this method is thermally stable, as there was minimal change in the neutrality points after heat treatment.

3. Conclusion

In summary, we utilized a thin layer of PEIE to induce n-doping in graphene films without inducing significant defects in their structure. Simultaneous use of this polymer in a back-gate FET device with Au contacts results in formation of two separate Dirac points in the I_d–V_{gs} curve, as indicative of a graphene p–n–p junction. In addition, PEIE acts as a barrier layer and limits further change in the electronic structure of graphene that typically arises from the adsorption of atmospheric dopants and results in atmospherically and thermally stable devices. Variation in the PEIE thickness and posttransfer treatment of CVD graphene films may result in p–n–p junctions with controlled position of double Dirac points and minimum drain-to-source conductivities.

4. Experimental Section

Graphene Synthesis: Monolayer graphene was grown on a 25 µm thick sheet of Cu foil (Alfa Aesar, item No. 14482) in a low pressure environment (≈800 mTorr) using CVD. The Cu substrates were placed inside a quartz tube in a CVD furnace and were annealed at 1000 °C in an Ar/H_2 (50/20 sccm) environment for 30 min to increase the Cu grain size. In the growth step, 35 sccm CH_4 was introduced for 20 min maintaining the same H_2 and Ar gas flow rate. Then, the furnace was shut down and the quartz tube pulled out of the hot area to allow rapid cool down to room temperature under the same gas flow rate.

Graphene Transfer: To transfer graphene, the Cu was etched in iron (III) chloride (30%) overnight and the graphene samples were treated with hydrochloric acid (10%) for 10 min, followed by washing in deionized water to remove contaminants from the graphene film.[31] The samples were then annealed in an inert environment at 200 °C overnight to remove any species that might be chemically and/or physically adsorbed on the graphene during the transfer process.[31] Extreme care was taken to minimize the introduction of defects during the transfer process.

PEIE Film Thickness: It was determined by spectroscopic ellipsometry using an Alpha SE tool (J. A. Woollam Co.). Ellipsometery spectra was measured on multiple spots at angle incidents of 60°–70° with a beam spot size of 40 mm^2 and they were analyzed using CompleteEASE 4.72 (J. A. Woollam Co.) by considering a single-layer model (without surface roughness) and Cauchy refractive index dispersion characteristics.

X-ray Photoelectron Spectroscopy: The data were acquired using a spectrophotometer (VG Scientific ESCALAB 210) with an Al Kα X-ray source ($h\upsilon = 1486.68$ eV). The survey scan spectra were collected at the BE of 0–1300 eV with a step size of 1 eV at a pass energy of 200 eV and a spot size of 400 µm. Each measurement was examined in at least three spots to ensure reproducibility. Thermo Advantage v4.54 Build 02750 was utilized for analysis of the collected spectra, where a shirley-type background was subtracted and 70% Gaussian–30% Lorentzian curve fitting was performed. O1s was utilized for calibration purposes through charge shifting the O1s peak from SiO_2 to BE of 533 eV.

Raman Spectroscopy: It was acquired in a Renishaw inVia microscope spectrometer. All spectra were excited with visible (532 nm) laser light and collected in the backscattering configuration with a laser power below 0.5 mW to avoid laser-induced heating. A 50x objective lens was used to focus the laser on the samples during the Raman measurements. All Raman peaks were fitted with Gaussian–Lorentzian line shapes to determine the peak position, linewidth, and intensity of the 2D and G Raman peaks.

Work Function: It was measured by Scanning Kelvin Probe (Besocke Delta Phi) to verify the doping of graphene by PEIE and gold contacts and the shift in their Fermi energy level. Kelvin Probe WF measurements were taken on three spots on each substrate. Average values and standard deviations were generated over these spots. A highly ordered pyrolytic graphite sample with a WF of 4.5 eV was used as the reference sample.[21]

Electrical Transport Data: It was measured using a probe station equipped with an HP 4156 semiconductor parameter analyzer under an inert atmosphere.

Acknowledgments

The authors are grateful for the support of Georgia Tech MRSEC and the NSF CMMI grant number 0927736. The authors wish to acknowledge Bernard Kippelen and Yinhua Zhou for the WF measurements.

Received: August 15, 2014
Revised: October 19, 2014
Published online:

[1] X. Du, I. Skachko, A. Barker, E. Y. Andrei, *Nat. Nanotechnol.* **2008**, *3*, 491.
[2] T. Ohta, A. Bostwick, T. Seyller, K. Horn, E. Rotenberg, *Science* **2006**, *313*, 951.
[3] K. S. Novoselov, A. K. Geim, S. V. Morozov, D. Jiang, Y. Zhang, S. V. Dubonos, I. V. Grigorieva, A. A. Firsov, *Science* **2004**, *306*, 666.
[4] H. Yamaguchi, J. Granstrom, W. Nie, H. Sojoudi, T. Fujita, D. Voiry, M. Chen, G. Gupta, A. D. Mohite, S. Graham, M. Chhowalla, *Adv. Energy Mater.* **2014**, *4*, 1300986.
[5] H. Sojoudi, S. Graham, *ECS J. Solid State Sci. and Technol.* **2013**, *2*, M17.
[6] M. I. Katsnelson, K. S. Novoselov, A. K. Geim, *Nat. Phys.* **2006**, *2*, 620.
[7] J. R. Williams, L. DiCarlo, C. M. Marcus, *Science* **2007**, *317*, 638.
[8] S. Masubuchi, S. Morikawa, M. Onuki, K. Iguchi, K. Watanabe, T. Taniguchi, T. Machida, *Jpn. J. Appl. Phys.* **2013**, *52*,110105.
[9] T. H. Yu, C. W. Liang, C. D. Kim, B. Yu, *Appl. Phys. Lett.* **2011**, *98*.
[10] T. Lohmann, K. von Klitzing, J. H. Smet, *Nano Lett.* **2009**, *9*, 1973.
[11] D. B. Farmer, Y.-M. Lin, A. Afzali-Ardakani, P. Avouris, *Appl. Phys. Lett.* **2009**, *94*, 213106.
[12] J. Baltazar, H. Sojoudi, S. A. Paniagua, et al., *Adv. Funct. Mater.* **2014**, *24*, 5147.
[13] S. A. Paniagua, J. Baltazar, H. Sojoudi, S. K. Mohapatra, et al., *Mater. Horizons* **2014**, *1*, 111.
[14] X. He, N. Tang, L. Gao, J. X. Duan, Y. W. Zhang, F. C. Lu, F. J. Xu, X. Q. Wang, X. L. Yang, W. K. Ge, B. Shen, *Appl. Phys. Lett.* **2014**, *104*, 143102.
[15] Y. D. Kim, M. H. Bae, J. T. Seo, Y. S. Kim, H. Kim, J. H. Lee, J. R. Ahn, S. W. Lee, S. H. Chun, Y. D. Park, *ACS Nano* **2013**, *7*, 5850.
[16] M. Z. Iqbal, S. Siddique, M. W. Iqbal, J. Eom, *J. Mater. Chem. C* **2013**, *1*, 3078.

© 2014 WILEY-VCH Verlag GmbH & Co. KGaA, Weinheim

[17] X. M. Wang, W. G. Xie, J. Chen, J. B. Xu, *ACS Appl. Mater. & Interfaces* **2014**, *6*, 3.
[18] H.-Y. Chiu, V. Perebeinos, Y.-M. Lin, P. Avouris, *Nano Lett.* **2010**, *10*, 4634.
[19] H. Sojoudi, J. Baltazar, L. M. Tolbert, C. L. Henderson, S. Graham, *ACS Appl. Mater. & Interfaces* **2012**, *4*, 4781.
[20] J. Baltazar, H. Sojoudi, S. A. Paniagua, J. Kowalik, S. R. Marder, L. M. Tolbert, S. Graham, C. L. Henderson, *J. Phys. Chem. C* **2012**, *116*, 19095.
[21] Y. Zhou, C. Fuentes-Hernandez, J. Shim, J. Meyer, A. J. Giordano, H. Li, P. Winget, T. Papadopoulos, H. Cheun, J. Kim, M. Fenoll, A. Dindar, W. Haske, E. Najafabadi, T. M. Khan, H. Sojoudi, S. Barlow, S. Graham, J.-L. Bredas, S. R. Marder, A. Kahn, B. Kippelen, *Science* **2012**, *336*, 327.
[22] I. Gierz, C. Riedl, U. Starke, C. R. Ast, K. Kern, *Nano Lett.* **2008**, *8*, 4603.
[23] G. Giovannetti, P. A. Khomyakov, G. Brocks, V. M. Karpan, J. van den Brink, P. J. Kelly, *Phys. Rev. Lett.* **2008**, *101*, 026803.
[24] P. A. Khomyakov, A. A. Starikov, G. Brocks, P. J. Kelly, *Phys. Rev. B* **2010**, *82*, 115437.
[25] S. Yamacli, *Comput. Mater. Sci.* **2014**, *81*, 607.
[26] Z. Klusek, P. Dabrowski, P. Kowalczyk, W. Kozlowski, W. Olejniczak, P. Blake, M. Szybowicz, T. Runka, *Appl. Phys. Lett.* **2009**, *95*, 113114.
[27] X. N. Shen, H. M. Wang, T. Yu, *Nanoscale* **2013**, *5*, 3352.
[28] C. Gong, G. Lee, B. Shan, E. M. Vogel, R. M. Wallace, K. Cho, *J. Appl. Phys.* **2010**, *108*, 123711.
[29] Y. P. Wu, W. Jiang, Y. J. Ren, W. W. Cai, W. H. Lee, H. F. Li, R. D. Piner, C. W. Pope, Y. F. Hao, H. X. Ji, J. Y. Kang, R. S. Ruoff, *Small* **2012**, *8*, 3129.
[30] A. Dahal, R. Addou, H. Coy-Diaz, J. Lallo, M. Batzill, *Apl Mater.* **2013**, *1*, 042107.
[31] H. Sojoudi, J. Baltazar, C. Henderson, S. Graham, *J. Vac. Sci. & Technol. B* **2012**, *30*, 041213.
[32] S. Bae, H. Kim, Y. Lee, X. Xu, J.-S. Park, Y. Zheng, J. Balakrishnan, T. Lei, H. R. Kim, Y. I. Song, Y.-J. Kim, K. S. Kim, B. Ozyilmaz, J.-H. Ahn, B. H. Hong, S. Iijima, *Nat. Nanotechnol.* **2010**, *5*, 574.
[33] A. Das, S. Pisana, B. Chakraborty, S. Piscanec, S. K. Saha, U. V. Waghmare, K. S. Novoselov, H. R. Krishnamurthy, A. K. Geim, A. C. Ferrari, A. K. Sood, *Nat. Nano* **2008**, *3*, 210.
[34] M. Kalbac, A. Reina-Cecco, H. Farhat, J. Kong, L. Kavan, M. S. Dresselhaus, *ACS Nano* **2010**, *4*, 6055.
[35] A. Nourbakhsh, M. Cantoro, B. Li, R. Mueller, S. De Feyter, M. M. Heyns, B. F. Sels, S. De Gendt, *Phys. Status Solidi-Rapid Res. Lett.* **2012**, *6*, 53.
[36] G. Rao, M. Freitag, H. Y. Chiu, R. S. Sundaram, P. Avouris, *ACS Nano* **2011**, *5*, 5848.
[37] W. X. Wang, S. H. Liang, T. Yu, D. H. Li, Y. B. Li, X. F. Han, *J. Appl. Phys.* **2011**, *109*, 07C501.
[38] H. Q. Zhou, C. Y. Qiu, F. Yu, H. C. Yang, M. J. Chen, L. J. Hu, Y. J. Guo, L. F. Sun, *J. Phys. D: Appl. Phys.* **2011**, *44*, 185404.
[39] I. Calizo, S. Ghosh, W. Bao, F. Miao, C. N. Lau, A. A. Balandin, *Solid State Commun.* **2009**, *149*, 1132.
[40] I. Calizo, F. Miao, W. Bao, C. N. Lau, A. A. Balandin, *Appl. Phys. Lett.* **2007**, *91*, 071913.
[41] B. Das, R. Voggu, C. S. Rout, C. N. R. Rao, *Chem. Commun.* **2008**, *41*, 5155.
[42] A. C. Ferrari, J. C. Meyer, V. Scardaci, C. Casiraghi, M. Lazzeri, F. Mauri, S. Piscanec, D. Jiang, K. S. Novoselov, S. Roth, et al., *Phys. Rev. Lett.* **2006**, *97*, 187401.
[43] L. M. Malard, M. A. Pimenta, G. Dresselhaus, M. S. Dresselhaus, *Phys. Rep.* **2009**, *473*, 51.
[44] Z. H. Ni, T. Yu, Z. Q. Luo, Y. Y. Wang, L. Liu, C. P. Wong, J. M. Miao, W. Huang, Z. X. Shen, *ACS Nano* **2009**, *3*, 569.
[45] K. S. Novoselov, F. Schedin, A. K. Geim, S. V. Morozov, E. W. Hill, P. Blake, M. I. Katsnelson, *Nat. Mater.* **2007**, *6*, 652.
[46] K. Yokota, K. Takai, T. Enoki, *Nano Lett.* **2011**.
[47] B. Guo, Q. Liu, E. Chen, H. Zhu, L. Fang, J. R. Gong, *Nano Lett.* **2010**,*10*, 4975.
[48] Y. C. Lin, C. Y. Lin, P. W. Chiu, *Appl. Phys. Lett.* **2010**, *96*, 133110.
[49] J. Park, W. H. Lee, S. Huh, S. H. Sim, S. B. Kim, K. Cho, B. H. Hong, K. S. Kim, *J. Phys. Chem. Lett.* **2011**, *2*, 841.
[50] W. C. Shin, S. Seo, B. J. Cho, *Appl. Phys. Lett.* **2011**, *98*, 153505.
[51] X. Wang, X. Li, L. Zhang, Y. Yoon, P. K. Weber, H. Wang, J. Guo, H. Dai, *Science* **2009**, *324*, 768.
[52] B. R. Matis, J. S. Burgess, F. A. Bulat, A. L. Friedman, B. H. Houston, J. W. Baldwin, *ACS Nano* **2012**, *6*, 17.
[53] B. R. Matis, B. H. Houston, J. W. Baldwin, *Phys. Rev. B* **2013**, *88*, 085441.
[54] R. Nouchi, K. Tanigaki, *Jpn. J. Appl. Phys.* **2011**, *50*, 070109.
[55] T. Mueller, F. Xia, M. Freitag, J. Tsang, P. Avouris, *Phys. Rev. B* **2009**, *79*, 245430.
[56] R. Golizadeh-Mojarad, S. Datta, *Phys. Rev. B* **2009**, *79*, 085410.
[57] A. Di Bartolomeo, F. Giubileo, S. Santandrea, F. Romeo, R. Citro, T. Schroeder, G. Lupina, *Nanotechnol.* **2011**, *22*, 275702.
[58] H. Xu, J. X. Wu, Y. B. Chen, H. L. Zhang, J. Zhang, *Chem.-Asian J.* **2013**, *8*, 2446.
[59] F. Schwierz, *Nat. Nanotechnol.* **2010**, *5*, 487.
[60] Z. Yan, Z. Z. Sun, W. Lu, J. Yao, Y. Zhu, J. M. Tour, *ACS Nano* **2011**, *5*, 1535.
[61] R. Wang, S. Wang, D. Zhang, Z. Li, Y. Fang, X. Qiu, *ACS Nano* **2011**, *5*, 408.
[62] B. Handel, B. Hahnlein, R. Gockeritz, F. Schwierz, J. Pezoldt, *Appl. Surf. Sci.* **2014**, *291*, 87.

© 2014 WILEY-VCH Verlag GmbH & Co. KGaA, Weinheim